Journal of Applied Electrochemistry (2006) 36:1433–1439
DOI 10.1007/s10800-006-9238-4

Rutile TiO_2-modified multi-wall carbon nanotubes in TiO_2 film electrodes for dye-sensitized solar cells

SUN LAE KIM[1], SONG-RIM JANG[1], R. VITTAL[1], JIWON LEE[2] and KANG-JIN KIM[1,*]
[1]*Division of Chemistry and Molecular Engineering, Korea University, Seoul, 136-713, Korea*
[2]*Samsung SDI, Co. Ltd., Gyeonggi-Do, 449-577, Korea*
*(*author for correspondence, tel.: + 82-2-3290-3127, fax: + 82-2-3290-3121, e-mail: kjkim@korea.ac.kr)*

Received 1 November 2005; accepted in revised form 5 September 2006

Key words: dye-sensitized solar cell, multi-wall carbon nanotube, open-circuit voltage, rutile TiO_2-modification, short-circuit photocurrent

Abstract

The beneficial influence of incorporation of acid-treated and rutile TiO_2 (r-TiO_2)-modified multi-wall carbon nanotubes (MWNTs) in TiO_2 films on photocurrent–voltage characteristics of dye-sensitized solar cells (DSSCs) was studied. Two different routes were adopted for the modification of acid-treated MWNTs (a-MWNTs) with r-TiO_2. The films and MWNTs were characterized by electron microscopy, energy dispersive X-ray spectroscopy, XRD and Raman spectroscopy. In the case of incorporation of a-MWNTs with r-TiO_2 modification, short-circuit photocurrent (J_{sc}) of the pertinent DSSC increased by 35% compared with that of a cell with bare TiO_2 film. The open-circuit voltage remained almost the same for all cases. The enhanced J_{sc} is explained by the increased surface area of the film, enhanced cluster formation of TiO_2 particles around a-MWNTs, and improved interconnectivity of TiO_2 particles in the presence of a-MWNTs.

1. Introduction

Carbon nanotubes constitute one of the four allotropic forms of carbon. Such tubes are in the form of a sheet rolled into a cylinder-like structure and may have single or multi walls. Carbon nanotubes have attracted intensive attention in many applications, such as field-emission displays [1], electrochemical energy storage devices [2], molecular electronic devices [3], nanotube actuators [4], and electrochemical capacitors [5] among others.

Inclusion of carbon nanotubes in an inorganic TiO_2 sol-gel matrix was reported by Vincent et al. [6]. Huang and Gao have immobilized rutile TiO_2 (r-TiO_2) on multi-wall carbon nanotubes (MWNTs) and studied the relevant growth behavior [7]. Ago and colleagues have fabricated photovoltaic devices using composites of MWNTs and conjugated polymers [8]. Usui et al. have prepared ionic gel electrolytes by dispersing MWNTs into ionic liquid electrolytes, and achieved higher energy conversion efficiency with corresponding dye-sensitized solar cells (DSSCs), relative to those using bare ionic liquid electrolytes [9].

It has been reported that the photovoltages of DSSCs fabricated with anatase and r-TiO_2 are comparable at one-sun intensity (100 mW cm^{-2}) [10, 11]. Compared to anatase TiO_2, r-TiO_2 has superior light scattering properties because of its higher refractive index and is chemically more stable and potentially cheaper to produce [12]. Higher light scattering properties are beneficial from the perspective of effective light harvesting. Hydrolysis of $TiCl_4$ is the process commonly used for obtaining highly porous r-TiO_2 films for DSSCs. However, analyses by intensity-modulated photocurrent spectroscopy along with scanning electron microscopic data suggest that electron transport is slower in the rutile layer than in the anatase layer due to differences in interparticle connectivity associated with particle packing density [10]. One possible way of achieving the promotion of electron transfer through r-TiO_2 film electrodes is to utilize carbon nanotubes, which also act as light scattering centers. The basis for this idea is the report by Stéphan et al. that introduction of MWNTs in poly(methyl methacrylate) polymers increased the conductivity of the composite by 9 orders of magnitude [13]. It has been reported that treating carbon nanotubes with a concentrated acid mixture of H_2SO_4 and HNO_3 [14–17] and of H_2SO_4 and $KMnO_4$ [18] results in introducing carboxylic acid groups to the nanotubes in addition to shortening them [19]. By analogy with the fact that carboxylic acid groups of Ru(II)-based dye molecules bond covalently to TiO_2 in DSSCs, it is assumed that MWNTs attached with carboxylic acid groups can adhere more strongly to TiO_2 particles than untreated MWNTs.

We have not found any reports on the influence of acid-treated MWNTs (a-MWNTs) on the photovoltaic properties of DSSCs. We have recently reported that incorporation of single-wall carbon nanotubes (SWNTs) in TiO_2 film increased the short-circuit photocurrent (J_{sc}) of DSSCs [20]. In this case the incorporation was irregular; SEM analyses indicated that SWNTs were not uniformly distributed in the TiO_2 film and that some portions of the SWNTs were not attached to the nanocrystalline TiO_2 particles.

In the present research we have preferred a-MWNTs and studied their beneficial influence, with and without r-TiO_2 modification, when incorporated in P25 TiO_2 films, on the photovoltaic properties of the pertinent DSSCs. Incorporation of MWNTs was intended owing to their relatively high conductivity (8 S cm^{-1} at room temperature [8]), and modification of MWNTs with r-TiO_2 was aimed at utilizing the latter's superior light scattering property relative to anatase TiO_2. Two types of investigation are presented in this paper. First, a-MWNTs were incorporated in P25 TiO_2 films. In the second investigation, r-TiO_2 was grown on a-MWNTs by two different methods using hydrolyzed $TiCl_4$, and these r-TiO_2-encapsulated nanotubes were incorporated in P25 films.

2. Experimental

Twenty mg of MWNTs (prepared by arc discharge, Iljin Nanotech, 90% purity) were oxidized in 30 ml of concentrated HNO_3 by refluxing for 6 h in a silicone oil bath maintained at 140 °C. The contents were filtered through a 200 nm pore size PTFE membrane. The filtrate was washed with a dilute NaOH solution and distilled water, followed by drying it in an oven at 100 °C. The resulting powder was designated as a-MWNTs.

In the first investigation, 0.5 mg of a-MWNT, which had been dispersed in a small amount of water, was mixed with 1.2 g of P25 to prepare TiO_2 colloidal mixture according to a procedure given elsewhere [21]. This colloidal mixture was coated on fluorine doped SnO_2 (FTO) conducting glass (Libbey-Owen-Ford Co.) by using the doctor blade technique, and annealed at 450 °C for 30 min in air.

In the second investigation, r-TiO_2 was grown on a-MWNTs prior to mixing them with P25. The growth was accomplished by two methods:

Method "a": 10 mg of a-MWNTs were suspended in 10 ml of 0.2 M hydrolyzed $TiCl_4$ solution in a vial and the contents were stirred for 3 days, centrifuged, washed with distilled water and ethanol in sequence, and dried at 100 °C for 16 h. The resulting powder was designated as r-TiO_2(0.2)/a-MWNTs.

Method "b" [7]: 10 mg of MWNTs were suspended in 7 ml of concentrated HNO_3 and refluxed for 6 h in a silicone oil bath maintained at 140 °C. The temperature of the bath was cooled to 60–70 °C and 7 ml of 2.0 M hydrolyzed $TiCl_4$ was rapidly injected into the contents under vigorous stirring condition. After 6 h the final products were centrifuged, washed with distilled water and ethanol in sequence, and dried at 100 °C for 16 h. The resulting powder was designated as r-TiO_2(2.0)/a-MWNTs.

About 0.5 mg each of r-TiO_2 immobilized a-MWNTs obtained from the two methods were dispersed separately in small amounts of water and mixed with 1.2 g of P25 to prepare TiO_2 colloidal mixtures. From these pasty TiO_2 colloidal mixtures, films were obtained on FTO conducting glass as described in the first investigation above.

For explanations in the following, we designate the TiO_2 film prepared in the first investigation as Film A, the one with r-TiO_2(0.2)/a-MWNTs as Film B, and that with r-TiO_2(2.0)/a-MWNTs as Film C. Nearly the same TiO_2 film thickness was maintained in all three cases, this being 18 μm. The reason for these thick films was to prevent MWNTs from protruding from the films, which otherwise could have caused a short circuit in the DSSCs. The TiO_2 films thus obtained were coated for 24 h at room temperature with dye in absolute ethanol containing 0.3 mM of $[RuL_2(NCS)_2]\cdot 2H_2O$, where L = 2,2′-bipyridine-4,4′-dicarboxylic acid. After the dye adsorption, additional non-bonded dye was removed by washing the dye-coated TiO_2 film with anhydrous ethanol. Thus a monolayer of dye on TiO_2 was ensured. Fabrication of DSSCs was accomplished by the method given elsewhere [21]. The electrolyte solution consisted of 0.6 M 1,2-dimethyl-3-hexylimidazolium iodide, 0.5 M 4-*tert*-butylpyridine, 0.1 M LiI, and 0.05 M I_2 in 3-methoxypropionitrile.

TEM micrographs of the annealed powders were obtained by a JEOL 1200EX to characterize the attachment of TiO_2 to MWNTs. Energy dispersive X-ray (EDX) spectra were recorded with a Hitachi S-4300 microscope to visualize the distribution of MWNTs in the TiO_2 film. FTIR and XPS spectra were obtained using a Bowman, Harman & Braun MB-series and an SSI 2803-S X-ray photoelectron spectrometer, respectively, to identify the formation of carboxylic acid groups on a-MWNTs. Raman spectra were obtained using a Jobin-Yvon T 64000 spectrophotometer to identify the attachment of r-TiO_2 to MWNTs. XRD measurements were carried out using an MAC Science Co. MO3XHF X-ray diffractomer with Cu Kα radiation. Scattering intensities of the films were measured by utilizing an Aminco-Bowman series-2 luminescence spectrometer with a solid film holder. Photocurrent–voltage curves were measured using a Keithley Model M236 source measure unit. A 300 W Xe lamp with an AM 1.5 filter (Oriel) was used to illuminate an active area of 0.4×0.5 cm of the TiO_2 electrode. An HP 8453A diode array spectrophotometer was used to estimate the amount of dye adsorbed to the TiO_2 films and for obtaining variable–potential spectra. Incident photon-to-current conversion efficiency (IPCE) was measured

with an Aminco-Bowman FA-256 luminescence spectrometer.

3. Results and discussion

FTIR and XPS spectra (not shown) identified the attachment of carboxylic acid groups to acid treated MWNTs (a-MWNTs). FTIR spectra of a-MWNTs showed a C=O peak of the COOH groups at 1730 cm^{-1} and a broad OH peak around 3400 cm^{-1}, in addition to a C=C peak of MWNTs at 1600 cm^{-1}. XPS data of a-MWNTs showed that the relative area of the peak at 289.0 eV [22] increased compared to that of untreated MWNTs due to the COOH groups. XPS analysis also indicated that the ratio of the atomic concentrations of O1*s* to C1*s* increased from essentially 0% to approximately 6% due to the oxidation of MWNTs by HNO_3. On the basis of these results, the presence of COOH groups in the a-MWNTs was confirmed. As a result of the shortening and simultaneous functionalization with COOH groups by nitric acid, a-MWNTs dispersed well in water [23]. Their good miscibility with water is beneficial for the fabrication of TiO_2 film electrodes; otherwise they need to be dispersed in an organic solvent such as DMF or *N*-methylpyrrolidine before being mixed with a P25 TiO_2 aqueous colloidal solution [20].

A crystalline phase of TiO_2 in the annealed powders of r-TiO_2(0.2)/a-MWNTs and r-TiO_2(2.0)/a-MWNTs was identified by XRD spectra. Figure 1 compares XRD patterns of r-TiO_2/a-MWNTs with pristine MWNTs. The peaks at 27.4, 36.1, 41.2 and 54.3° (JCPDS 21-1276) in Figure 1(a, b) clearly represent the crystalline phase of the immobilized TiO_2 to be rutile. A shoulder possibly arising from a-MWNTs is discernible at about 26.1° in Figure 1(a, b), but is slightly shifted from the corresponding peak of pristine MWNTs at 25.7° (Figure 1(c)) due to the changes occurring during the refluxing process in concentrated HNO_3 [7].

A TEM image in Figure 2(a) illustrates a-MWNT surrounded by TiO_2 particles of P25. The image was obtained from annealed powder, which was produced from a mixture of P25 and a-MWNTs, for portraying the degree of attachment of P25 particles to a-MWNTs. Figure 2(b, c) depict TEM images of annealed powders of r-TiO_2(0.2)/a-MWNTs and r-TiO_2(2.0)/a-MWNTs, respectively. Unlike the loose coverage of TiO_2 particles of P25 on the a-MWNT in Figure 2(a), a wrapping of the tubes by r-TiO_2 particles is observed in Figure 2(b, c), indicating that the coverage on a-MWNTs with r-TiO_2 particles strongly depends on the preparation method of the composite with TiO_2 (P25 or rutile) and a-MWNTs. It is interesting to note that the TiO_2 assumes needle-like structure in Figure 2(b) and peanut-like structure in Figure 2(c).

The a-MWNTs in TiO_2 colloidal mixtures essentially remained stable after annealing at 450 °C for 30 min in air. Their distribution in the TiO_2 films was visualized by EDX analysis as shown in Figure 3, which shows the typical mapping images of titanium, oxygen and carbon of Film B, while the P25 film did not reveal the mapping image of carbon. The results indicate relatively well-distributed a-MWNTs in the Film B. Similar mapping images to those of Film B were obtained for Films A and C.

As a supplementary to TEM, Raman spectroscopy was used to study adherence of r-TiO_2 particles to MWNTs. Figure 4(A) compares Raman spectra of r-TiO_2 immobilized a-MWNTs with that of pristine MWNTs in the region between 120 and 1800 cm^{-1}. The Raman spectra confirm that $TiCl_4$-produced TiO_2

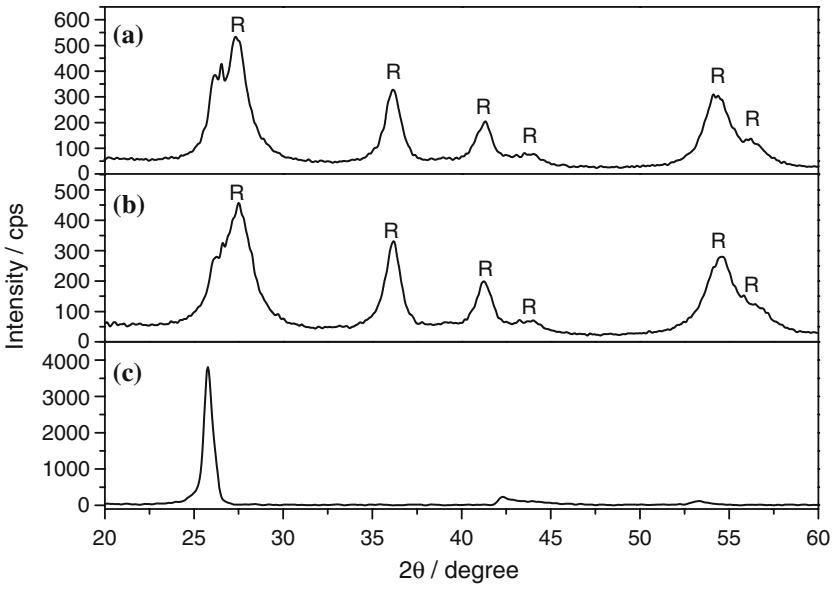

Fig. 1. XRD patterns of powders of (a) rutile TiO_2 (r-TiO_2)(0.2)/acid-treated MWNTs (a-MWNTs), (b) r-TiO_2(2.0)/a-MWNTs, and (c) pristine multi-wall carbon nanotubes (MWNTs). R denotes rutile. All samples were annealed at 450 °C for 30 min in air.

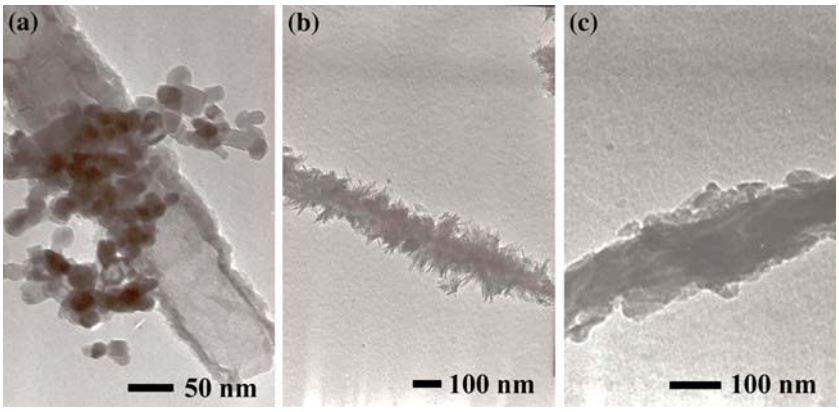

Fig. 2. TEM images of annealed powders of (a) acid-treated multi-wall carbon nanotube (a-MWNT) mixed with P25 particles, (b) rutile TiO_2 (r-TiO_2)(0.2)/a-MWNTs, and (c) r-TiO_2(2.0)/a-MWNTs.

crystallizes as rutile on a-MWNTs [12], regardless of the concentration of $TiCl_4$. In Figure 4(B), an expanded portion of Figure 4(A), the G-bands pertaining to the E_{2g} mode of MWNTs of r-TiO_2(0.2)/a-MWNTs and r-TiO_2(2.0)/a-MWNTs powders show blue-shifts by 4 and 7 cm^{-1}, respectively, with respect to that of pristine MWNTs at about 1557 cm^{-1} [24]. These blue-shifts can be attributed to the strain effects [25] at the a-MWNT/TiO_2 interfaces, which may influence the vibrational frequencies. Incidentally, Figure 4(C), expansion of Figure 4(A) in the 400–700 cm^{-1} region, reveals that the E_g and A_{1g} bands of r-TiO_2(2.0)/a-MWNTs are slightly blue-shifted relative to those of r-TiO_2(0.2)/a-MWNTs. All these Raman spectral changes of a-MWNTs are due to the adherence of r-TiO_2 particles to a-MWNTs.

Figure 5 shows *J–V* curves of DSSCs made by incorporating a-MWNTs, with and without r-TiO_2 modification, in the TiO_2 films, compared with that of a cell fabricated with P25 film only. The results are summarized in Table 1. Compared to a cell fabricated with P25 film only, the cell with Film A shows a higher J_{sc} by about 12%. Similarly the cells with Films B and C show J_{sc} improvements of about 27 and 35%, respectively. However, there are hardly any changes in open-circuit voltage (V_{oc}) and fill factor (FF) of the four cells. As a result of mainly J_{sc} enhancements, the overall energy conversion efficiency (η) has increased by 17, 24, and 38% for the cells prepared with Films A, B and C, respectively, with respect to that of the cell made with P25 film only.

The essential reason for the enhanced J_{sc} is attributed to increased surface area of the TiO_2 films in the presence of a-MWNTs. This can be verified by measuring absorbance of desorbed dye from a TiO_2 film. Enhanced quantity of dye adsorption is indicative of enhanced surface area of TiO_2 film for a monolayer of dye on the TiO_2 particles. Absorbance measurements of the desorbed dye from TiO_2 films with and without a-MWNTs in Figure 6 indicate increased dye adsorption by about 40% in the case of Film A, and by 57 and 71% in the cases of Films B and C, respectively, compared to that of the unmodified P25 film. This suggests that the surface area of TiO_2 films for dye adsorption has increased in the order of surface area of P25 < Film A < Film B < Film C. The J_{sc} increases are consistent with this order of increase of surface area. The increased surface area of TiO_2 films with the incorporation of a-MWNTs may be due to additional adsorption sites gained from the adherence of TiO_2 particles to a-MWNTs (Figure 1(a)), that are otherwise not available when TiO_2 particles aggregate themselves in the P25 film. Because of the fine distribution of a-MWNTs in the TiO_2 films, as can be understood from Figure 3, a better dispersion of TiO_2 particles in the film can be

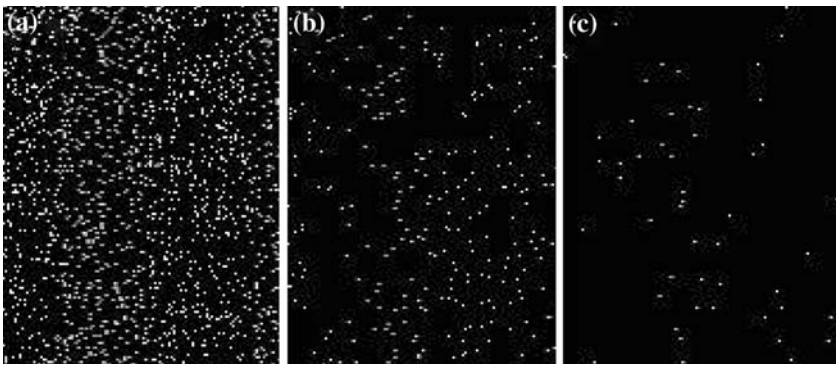

Fig. 3. EDX mapping images of Film B: (a) titanium, (b) oxygen, and (c) carbon.

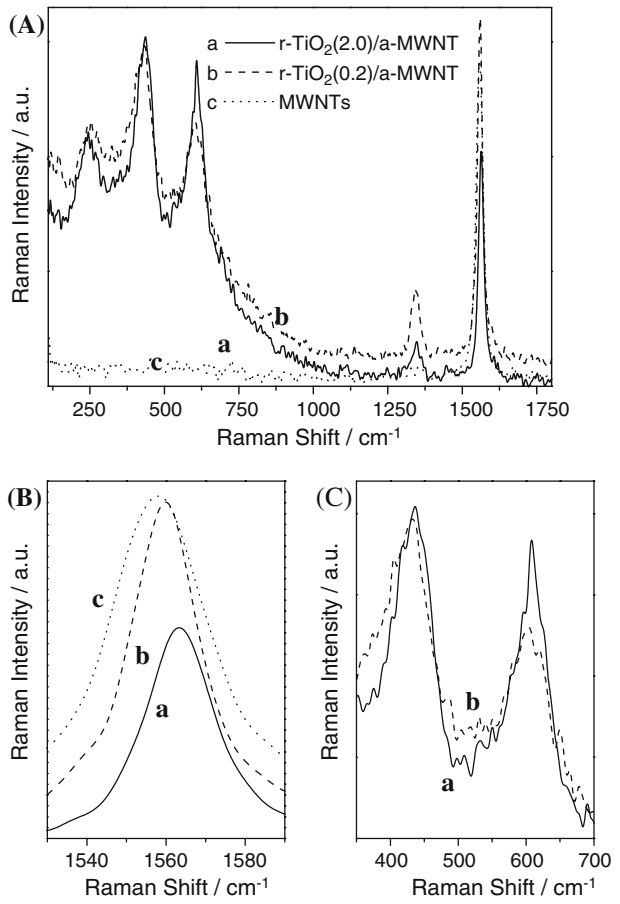

Fig. 4. (A) Raman spectra of (a) rutile TiO_2 (r-TiO_2)(2.0)/acid-treated multi-wall carbon nanotubes (a-MWNTs) (solid curve), (b) r-TiO_2(0.2)/acid-treated multi-wall carbon nanotubes (a-MWNTs) (broken curve), and (c) pristine-MWNTs (dotted curve); (B) Expansion of (A) in the region of 1500–1600 cm^{-1}; (C) Expansion of (A) in the region of 350–700 cm^{-1}.

visualized and hence additional adsorption sites for the dye. We have verified in our previous work [26] that the Ru(II) dye does not adsorb onto SWNTs. Therefore, we do not attribute the increased surface area to a-MWNTs. The adsorption of the dye is assumed to

Table 1. Photovoltaic parameters of dye-sensitized solar cells (DSSCs)[a,b] made with films A, B and C and with a bare P25 film

Electrode[c]	J_{sc}/mA cm^{-2}	V_{oc}/V	FF	η/%
P25	7.41	0.69	0.56	2.88
Film A	8.38	0.68	0.59	3.40
Film B	9.44	0.68	0.56	3.60
Film C	10.02	0.69	0.58	4.04

[a]Radiant power was 100 mW cm^{-2}.
[b]Electrolyte solution consisted of 0.6 M 1,2-dimethyl-3-hexylimidazolium iodide, 0.5 M 4-*tert*-butylpyridine, 0.1 M LiI, and 0.05 M I_2 in 3-methoxypropionitrile.
[c]Films A, B, and C were prepared each with 1.2 g of P25 added respectively with 0.5 mg of a-MWNTs, r-TiO_2(0.2)/a-MWNTs, and r-TiO_2(2.0)/a-MWNTs.

be on TiO_2 particles. The adsorption sites apparently increased further with uniform immobilization of r-TiO_2 on a-MWNTs, with respect to Film A. The difference in Films B and C can be rationalized by considering that the peanut-like r-TiO_2 particles of Film C (Figure 1(c)) can lead to a larger surface area for the dye adsorption than the needle-like r-TiO_2 particles of Film B (Figure 1(b)).

The J_{sc} enhancements are supported by unfailing higher IPCE values at all wavelengths over the visible region (Figure 7(a)). The J_{sc} increase also arises from enhanced light scattering by the TiO_2 films with a-MWNTs. Figure 7(b) shows that the TiO_2 films with a-MWNTs scatter more light intensity at the angle of 10° over the 400–800 nm region than the P25 film. The reason for this may be favorable TiO_2 cluster formation induced by a-MWNTs in the films in the order of that of P25 < Film A < Film B < Film C, again in agreement with the order of the J_{sc} increase. The enhanced light scattering of Films B and C, compared to that of the film P25 and Film A can be accounted for the higher light scattering properties of r-TiO_2 on a-MWNTs. The variation in morphology and amount of r-TiO_2 on a-MWNTs, caused by the one order difference in $TiCl_4$

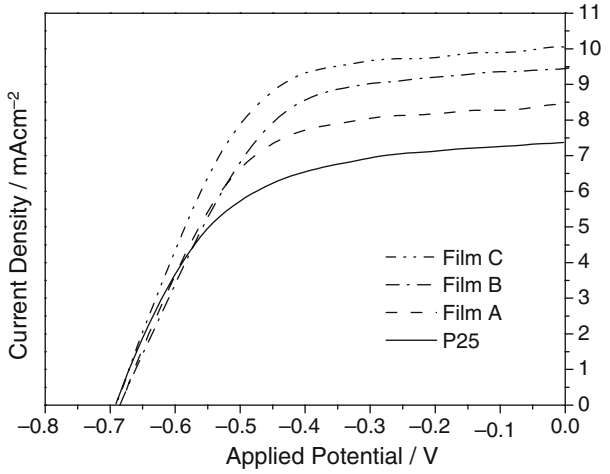

Fig. 5. J–V curves of dye-sensitized solar cells (DSSCs) prepared with Films A, B, C, and unmodified P25 film.

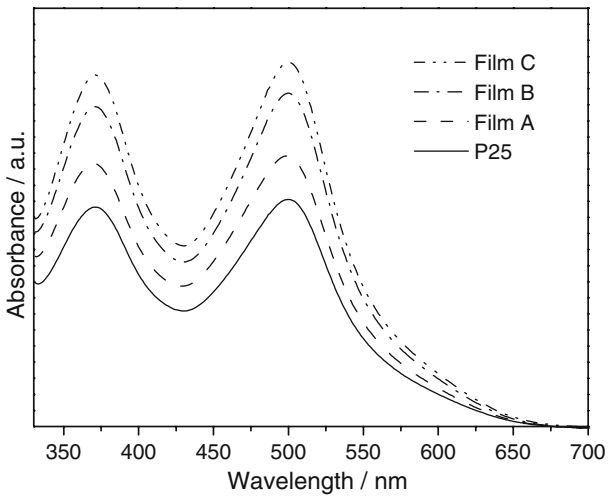

Fig. 6. Absorption spectra of dye desorbed from TiO_2 films with and without acid-treated multi-wall carbon nanotubes (a-MWNTs).

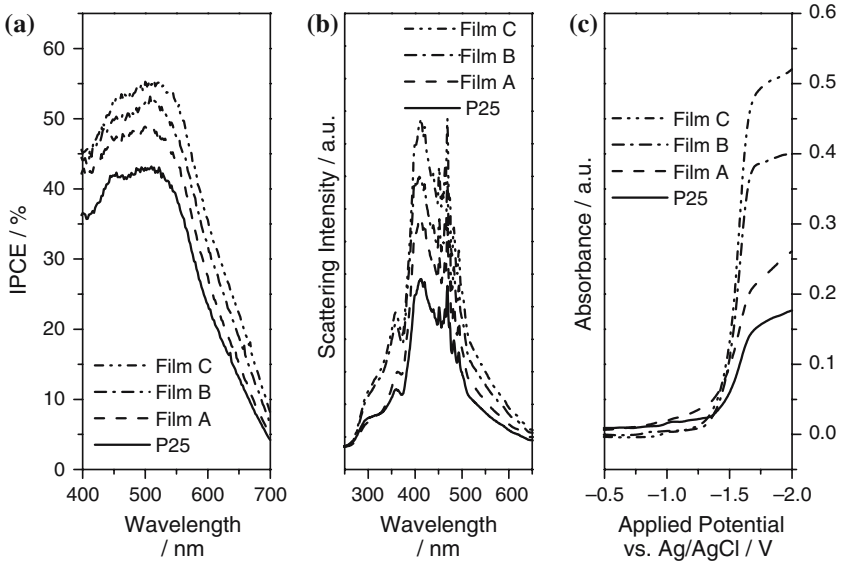

Fig. 7. (a) Action spectra of dye-sensitized solar cells (DSSCs) corresponding to the *J–V* curves in Figure 5, (b) light scattering intensities measured at 10° from the light source, and (c) absorbance measured at 800 nm as a function of applied potential at a scan rate of 5 mV s^{-1}.

concentration used, can explain the increased light scattering of Film C compared with that of Film B.

The J_{sc} enhancement can also be explained by the increase in interconnection among the TiO_2 particles in the TiO_2 films prepared with a-MWNTs. Formation of a-MWNT-induced clusters, as mentioned already, enables increase in interconnection among the TiO_2 particles in the film, relative to that among the particles in the film without a-MWNTs. The increased interconnectivity in turn increases the electrical conductivity of the film in the presence of a-MWNTs. We have recently verified through electrochemical impedance spectroscopy that the resistance of SWCN-incorporated TiO_2 film decreased conspicuously by a factor of three compared to that of the unmodified TiO_2 film [27]. We have also noted that MWNTs are two-dimensional electrical conductors, while infinitely long SWNTs exhibit one-dimensional conduction [27]. In addition to improved interconnectivity among TiO_2 particles in the films in the presence of MWNTs, the anchoring of TiO_2 particles to nanotubes can promote charge separation, owing to the fact that carboxylic acid groups of a-MWNTs are also able to attach themselves to TiO_2 particles.

Using the spectroscopic technique developed by Rothenberger et al. [28], further explanation is provided for the J_{sc} enhancements. Figure 7(c) shows the absorbance at 800 nm as a function of applied potential with reference to an Ag/AgCl electrode of film electrodes A, B and C, and of an unmodified P25 film electrode, in acetonitrile containing 0.2 M tetrabutylammonium perchlorate and 0.5 M $LiClO_4$. It can be seen that the absorbances in the case of Films A, B and C are clearly more than that of a bare TiO_2 film. Since absorbance is proportional to the free electron density in the conduction band of TiO_2 [28], the implication is a higher electron transport in Films A, B and C. This suggests that the surface electron trap sites are possibly blocked by the improved interconnectivity among TiO_2 particles. The absorbance pattern of Films A, B and C is consistent with their respective J_{sc} enhancements. Support for the blocking of surface electron trap sites is gained from the transient photocurrents of the cells made with Film B and P25 film, as typically shown in Figure 8. The figure shows the rise and fall of the J_{sc} recorded during one on-off cycle of illumination at 100 mW cm^{-2}. The time required for the fall of the J_{sc} by 90% in the case of DSSC with Film B is estimated to be faster by about 0.15 s than that in the case of the cell with P25 film. Similarly, the J_{sc} of the cell made with Film C decreased faster by about 0.12 s compared to that of the cell with P25 film (figure not shown). Electrons trapped in the surface states appear to be responsible for the slower photocurrent response in the case of the DSSC with bare P25 film [29, 30].

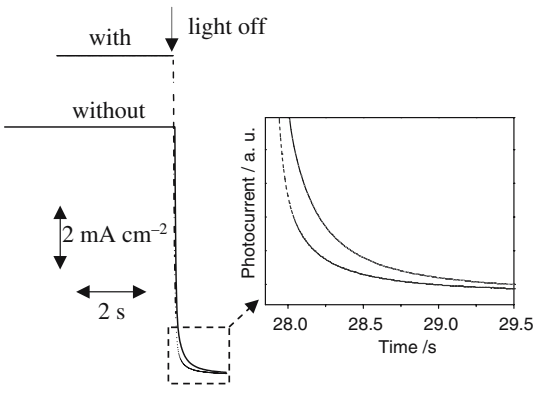

Fig. 8. Transient short-circuit photocurrent (J_{sc}) of dye-sensitized solar cells (DSSCs) prepared with (dotted line) and without (solid line) rutile TiO_2 (r-TiO_2)(0.2)/acid-treated multi-wall carbon nanotubes (a-MWNTs) at 100 mW cm^{-2}.

It is to be emphasized here that the performance of the cell is not optimized with regard to film thickness, dye purification and device architecture. This study focused on the influence of a-MWNTs and r-TiO_2/a-MWNTs, when incorporated in P25 TiO_2 film, on the photovoltaic properties of the corresponding DSSCs. Comparative measurements were made in this regard with reference to a cell without a-MWNTs.

4. Conclusions

Incorporation of acid-treated multi-wall carbon nanotubes (a-MWNTs) and of r-TiO_2-modified a-MWNTs in P25 TiO_2 films yields considerably increased J_{sc} with the same open-circuit voltage and fill factor for the pertinent dye-sensitized solar cells, with respect to the unmodified cell. The essential reason for the J_{sc} enhancement is attributed to increased surface area of the films fabricated in the presence of a-MWNTs. The J_{sc} increase also arises from more favorable cluster formation in P25 TiO_2 films in the presence of a-MWNTs or r-TiO_2/a-MWNTs than that in the absence of them. Improved interconnectivity among TiO_2 particles in the presence of the a-MWNTs is seen as another reason for the J_{sc} enhancements. Furthermore, prior adherence of r-TiO_2 to a-MWNTs results in higher J_{sc} increases compared to the case of bare a-MWNTs in TiO_2 film. The J_{sc} of the cell with a film having a-MWNTs immobilized by r-TiO_2 using 2.0 M $TiCl_4$ is larger than that of a similar cell where 0.2 M $TiCl_4$ is used, which is attributed to the morphology of r-TiO_2 on a-MWNTs. The J_{sc} enhancements are consistent with the increase in dye adsorption, light scattering and potential-dependent optical absorbance of the respective cells.

Acknowledgements

This work was supported by the Innovative Cluster Program of Seoul and by the Sol-Gel Innovation Project of the Ministry of Commerce, Industry and Energy in Korea.

References

1. W.A. De Heer, A. Chatelain and D. Ugarte, *Science* **270** (1995) 1179.
2. G. Che, B.B. Lakshmi, E.R. Fisher and C.R. Martin, *Nature* **393** (1998) 346.
3. S.J. Tans, A. Verschueren and C. Dekker, *Nature* **393** (1998) 49.
4. R.H. Baughman, C. Cui, A.A. Zakhidov, Z. Iqbal, J.N. Barisci, G.M. Spinks, G.G. Wallace, A. Mazzoldi, D. De Rossi, A.G. Rinzler, O. Jaschinski, S. Roth and M. Kertesz, *Science* **284** (1999) 1340.
5. C. Niu, E.K. Sichel, R. Hoch, D. Moy and H. Tennent, *Appl. Phys. Lett.* **70** (1997) 1480.
6. P. Vincent, A. Brioude, C. Journet, S. Rabaste, S.T. Purcell, J. Le Brusq and J.C. Plenet, *J. Non Crystalline Solids* **311** (2002) 130.
7. Q. Huang and L. Gao, *J. Mater. Chem.* **13** (2003) 1517.
8. H. Ago, K. Petritsch, M.S.P. Shaffer, A.H. Windle and R.H. Friend, *Adv. Mater.* **11** (1999) 1281.
9. H. Usui, H. Matsui, N. Tanabe and S. Yanagida, *J. Photochem. Photobiol. A: Chem.* **164** (2004) 97.
10. N.-G. Park, J. van de Lagemaat and A.J. Frank, *J. Phys. Chem. B* **104** (2000) 8989.
11. N.-G. Park, G. Schlichthörl, J. van de Lagemaat, H.M. Cheong, A. Mascarenhas and A.J. Frank, *J. Phys. Chem. B* **103** (1999) 3308.
12. K.-J. Kim, K.D. Benkstein, J. van de Lagemaat and A.J. Frank, *Chem. Mater.* **14** (2002) 1042.
13. C. Stéphan, T.P. Nguyen, B. Lahr, W. Blau, S. Lefrant and O. Chauvet, *J. Mater. Res.* **17** (2002) 396.
14. Z. Liu, Z. Shen, T. Zhu, S. Hou, L. Ying, Z. Shi and Z. Gu, *Langmuir* **16** (2000) 3569.
15. X. Nan, Z. Gu and Z. Liu, *J. Colloid Interface Sci.* **245** (2002) 311.
16. J. Liu, A.G. Rinzler, H. Dai, J.H. Hafner, R.K. Bradley, P.J. Boul, A. Lu, T. Iverson, K. Shelimov, C.B. Huffman, F. Rodriguez-Macias, D.T. Colbert and R.E. Smalley, *Science* **280** (1998) 1253.
17. K. Esumi, M. Ishigami, A. Nakajima, K. Sawada and H. Honda, *Carbon* **34** (1996) 279.
18. H. Hiura, T.W. Ebbesen and K. Tanigaki, *Adv. Mater.* **7** (1995) 275.
19. T. Saito, K. Matsushige and K. Tanaka, *Physica B* **323** (2002) 280.
20. K.-H. Jung, J.S. Hong, R. Vittal and K.-J. Kim, *Chem. Lett.* **31** (2002) 864.
21. M.G. Kang, N.-G. Park, S.H. Chang, S.H. Choi and K.-J. Kim, *Bull. Korean Chem. Soc.* **23** (2002) 140.
22. H. Ago, T. Kugler, F. Cacialli, W.R. Salaneck, M.S.P. Shaffer, A.H. Windle and R.H. Friend, *J. Phys. Chem. B* **103** (1999) 8116.
23. M.S.P. Shaffer, X. Fan and A.H. Windle, *Carbon* **36** (1998) 1603.
24. J.M. Holden, P. Zhou, X.-X. Bi, P.C. Eklund, S. Bandow, R.A. Jishi, K.D. Chowdhury, G. Dresselhaus and M.S. Dresselhaus, *Chem. Phys. Lett.* **220** (1994) 186.
25. C.Y. Xu, P.X. Zhang and L. Yan, *J. Raman Spectrosc.* **32** (2001) 862.
26. K.-H. Jung, S.-R. Jang, R. Vittal, D. Kim and K.-J. Kim, *Bull. Korean Chem. Soc.* **24** (2003) 1501.
27. J.-C. Charlier and J.-P. Issi, *Appl. Phys. A* **67** (1998) 79.
28. R. Rothenberger, D. Fitzmaurice and M. Grätzel, *J. Phys. Chem.* **96** (1992) 5983.
29. K. Schwartsburg and F. Willig, *Appl. Phys. Lett.* **58** (1991) 2520.
30. X. Qian, D. Qin, Q. Song, Y. Bai, T. Li, X. Tang, E. Wang and S. Dong, *Thin Solid Films* **385** (2001) 152.